Impact of stress-induced anisotropy caused by salt bodies on depth imaging: a synthetic case study

Adam Koesoemadinata, Ran Bachrach, Andrey Bakulin, Marta Woodward and Konstantin S. Osypov, WesternGeco*

Summary

As anisotropic depth imaging is widely used in the industry, anisotropic velocity models are routinely being constructed and applied. However, the degree of accuracy of the anisotropic velocity model needed to correctly position the horizons is not well defined. To that end, we tested four anisotropic parameter estimation scenarios and performed depth imaging using a realistic synthetic sedimentary seismic data that included an irregularly shaped salt body. Although similar images derived from the data using those four different anisotropic input models were obtained, a quantitative analysis indicates that systematic differences do exist. They enable us to relate the degree of accuracy needed in the image to the effort needed to build the anisotropic velocity model.

Introduction

In seismic exploration, common-image-point (CIP) tomography has become a standard tool for seismic depth imaging. CIP tomography continues to improve its capability including dealing with anisotropic VTI and TTI models as exploration demands increase (Woodward et. al, 2008). However, while determining an anisotropic velocity model in depth is essential to correctly position reflectors in depth and improve the clarity of the imaged reflectors, anisotropic model estimation becomes difficult in areas where complex geological structure may cause lateral anisotropic heterogeneity. Recently, Sengupta et al. (2009) showed how to generate anisotropic models in the presence of salt bodies using geomechanical principles. Geomechanical modeling indicated that significant salt-induced velocity anisotropy variations are expected in the sediments surrounding the salt body.

In this paper, we explore the sensitivity of depth imaging to various anisotropic (ε and δ) models. We use a realistic 2.5D synthetic anisotropic velocity model where salt-induced lateral anisotropy changes are present. The model was generated using geomechanical methods, following the same technique presented by Sengupta et al. (2009). We simulated a seismic survey using elastic anisotropic finite-difference modeling, and imaged the data using the following anisotropy models that were constructed based on the following realistic scenarios; a 1D anisotropic model that is built based on a single profile (assumed to be known from checkshot data), a 2D anisotropic model, an interpolated profile derived from two wells at two different locations, and a anisotropic model generated by using inaccurate third-order elasticity (TOE) parameters. For the last model, the scenario assumed that we can simulate the stresses using geomechanics, but there are errors in mapping stress changes to velocity changes. As our goal is to investigate the role of lateral heterogeneity in the anisotropy and to avoid subsalt imaging issues, we focus our attention to the sediments above the salt.

Synthetic anisotropic model

Sengupta et al. (2009) presented an application of 3D geomechanical modeling for anisotropic parameter estimation. A synthetic model with an irregularly shaped salt body was created based on a real 3D seismic image from a survey in the Gulf of Mexico. Sengupta et al. showed that the presence of irregularly shaped salt gives rise to large deviatoric stresses that can generate significant anisotropic velocity anomalies in the sediments surrounding the salt. The 3D stress and the velocity anisotropy are related. The basic idea is that stress-induced anisotropy can be represented to a first-order approximation by TOE elasticity theory (Sarkar et al., 2003; Prioul et al., 2004). In general the changes in the stiffness are linear with changes in stress:

$$C(\sigma_0 + \Delta\sigma) \approx C(\sigma_0) + \left.\frac{\partial C}{\partial \sigma}\right|_{\sigma_0} \Delta\sigma \qquad (1)$$

where the stress sensitivity coefficients are related to the strain sensitivity coefficients, and can be measured in the lab.

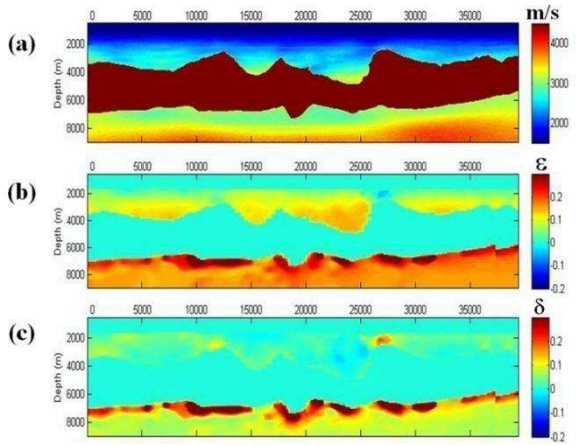

Figure 1: Anisotropic model used in this study in terms of (a) Vertical Vp, (b) ε, and (c) δ.

Synthetic forward modeling

Figure 1 shows our anisotropic model in terms of vertical velocity (Vp), and Thomsen's parameters ε and δ (Thomsen, 1986). The model consists of a water layer, a salt body, and the sediment zones above and below the salt. The vertical S-wave and density model that correspond to realistic Vp/Vs ratio and empirical velocity-density transform were also generated (not shown here). The

model was created by using the geometry of a real salt body in the Gulf of Mexico. Stresses and strains were computed using finite-element geomechanical modeling. In the geomechanical model, we calculated stress perturbation on top of the smooth VTI background. See Sengupta et al (2009) for more details. Note that the lateral anisotropy variations induced by the salt are clearly visible in the model. To generate reflectors we superposed small-scale perturbation on the density P-wave and S-wave velocity derived from the image of the true data. In addition, we embedded two horizontal reflectors in the model above and below the salt to better quantify the imaging results as will be discussed later.

We simulated seismic data using full elastic anisotropic finite-difference modeling. The grid size was specified to be 12.5 m. A split spread configuration was employed with a 25-m shot interval. The pressure response receivers were laid out along the line with 12.5-m interval. An explosive source with a 10-Hz central frequency Ricker wavelet was used for the simulation.

Ray-based reflection tomography

The ray-trace-based reflection tomography is based on the simple assumption that, if the velocity model is correct, the reflectors for all offset in the prestack migrated gathers should be flat. Figure 2 is a schematic of the ray-based tomography workflow that we used. The process starts with prestack (Kirchhoff) depth migration (PSDM) using our initial velocity model. Then, an auto-picker picks the reflectors on the PSDM gathers and calculates the residual moveout (RMO). A ray tracer traces the source-receiver rays corresponding to the reflector picks through the model to generate equations that relate changes in the model to changes in the RMO. These equations are solved to produce velocity updates that minimize the RMO. More details can be found in Woodward et al. (2008). Our initial model was a 1D velocity profile representing the sedimentary velocity depth trend over the area. We used tomography to change Vp only of the sediment above the salt and we held the anisotropic parameters fixed.

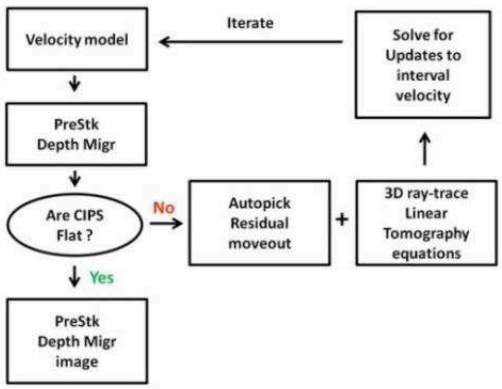

Figure 2: Tomography workflow (Woodward et. al., 2008).

At every iteration of tomography, the top salt horizon was re-picked because the sediment velocity was updated. We found that three iterations were sufficient to flatten the reflections. Tools for migrating/remigrating the top salt horizon, as well as for RMO QC were used in this iterative process.

Considerable care was taken in differentiating coherent noise from dipping reflectors caused by the RMO. We had to exclude the salt sediment interface refraction zones from the gathers. We also limited the incident angle for the reflection picking and RMO calculation to 50^{o}. This was to remove complications from the NMO stretch effect and prismatic waves.

Anisotropic input models

In Figure 3, we present the four different anisotropic input models used in our depth test. Model 1 (Figures 3a, 4a), is the true model that we created from the geomechanical modeling. Model 2 (Figures 3b, 4b), is a 1D anisotropic model taken from location 25000 m on the actual model and extrapolated laterally. Model 3 (Figures 3c, 4c), is a 2D interpolated anisotropic model following the scenario if we have two wells at 7500 m and 25000 m locations, and from them we extract anisotropy information and create 2D anisotropy profile by simple interpolation. Model 4 (Figures 3d, 4d) is, an anisotropic model similar to the actual model but it was generated using inaccurate elastic parameters. This model has similar general trend in ε as the actual model, but the magnitude is slightly different and the δ is quite different. In addition, we also ran the tomography using Model 5 (Figures 3e, 4e), an isotropic model assumption, for comparison.

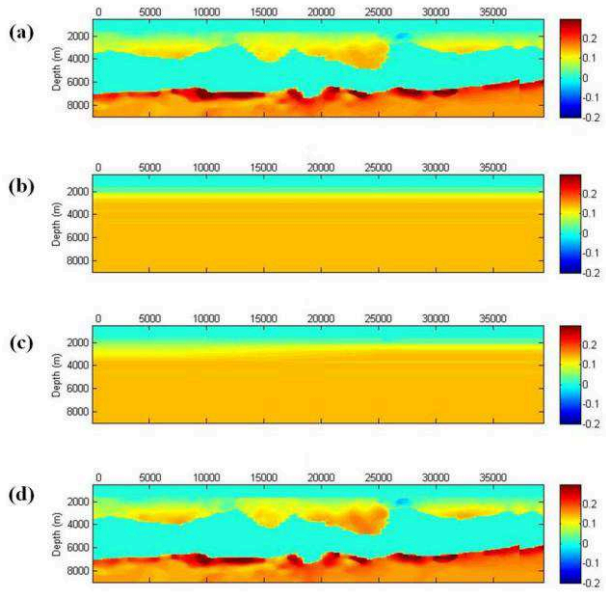

Figure 3: ε of (a) Model 1, (b) Model 2, (c) Model 3, and (d) Model 4.

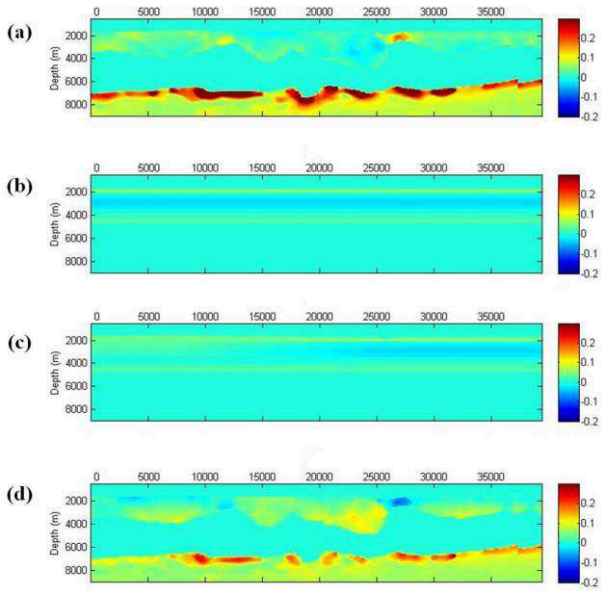

Figure 4: δ of (a) Model 1, (b) Model 2, (c) Model 3, and (d) Model 4.

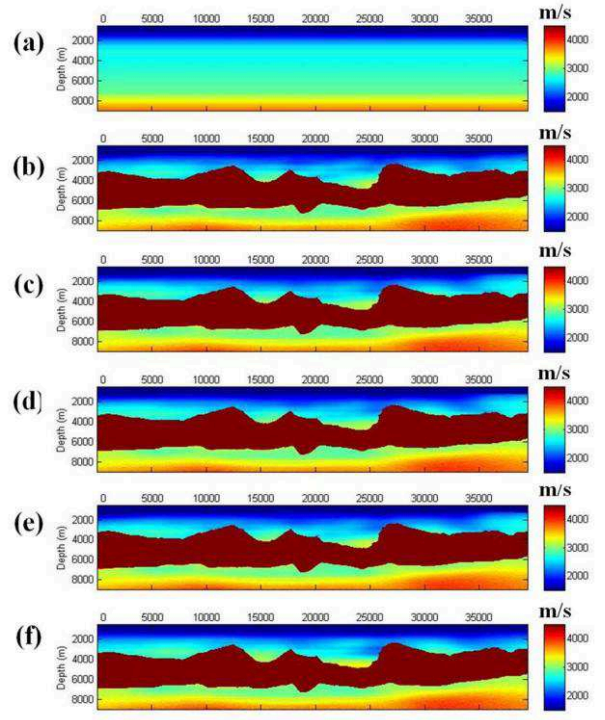

Figure 5: (a) Vertical velocity of initial model. Vertical velocities from tomography using (b) Model 1, (c) Model 2, (d) Model 3, (e) Model 4, and (f) Model 5.

Results

Figures 5 to 9 summarize the study results. Figure 5 shows the vertical velocity comparison obtained from tomography for all the models. Figure 6 shows the corresponding comparison of differences with respect to the actual model vertical velocity. It is clear the use of anisotropic model constraints produces a significantly different result compared to the isotropic assumption. However, the differences among the anisotropic scenarios are subtle except in a small area in the mid-section near the top salt where using the actual anisotropy model gives better velocity estimation.

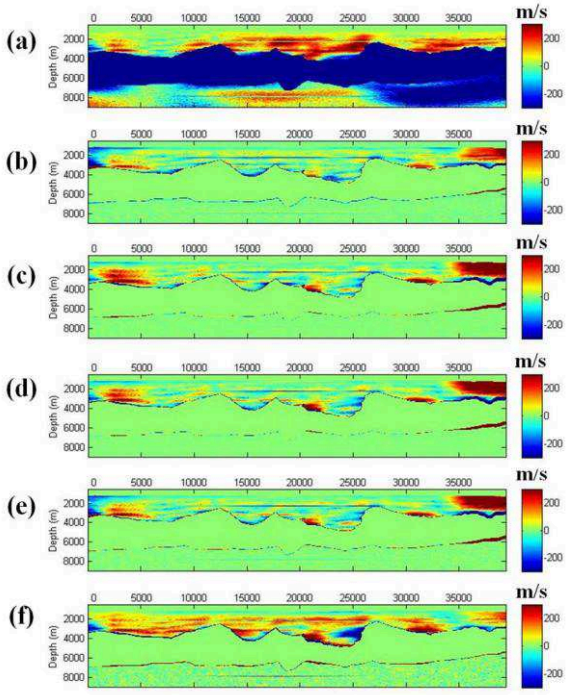

Figure 6: (a) Differences between vertical velocity of actual model and vertical velocity of initial model. Differences between vertical velocity of actual model and vertical velocity from tomography using (b) Model 1, (c) Model 2, (d) Model 3, (e) Model 4, and (f) Model 5.

Figure 7(b) shows the migrated stack obtained by using the actual velocity model. It is overlaid with horizons picks from the actual velocity model. Those picks are shown by red lines. The horizons are the water bottom, the horizontal layer above salt, the top salt, the base salt, and the horizontal layer below the salt. There is a perfect match between the actual velocity model and its corresponding migrated stack, as we expected. Figure 8 shows horizon picks from the migrated stacks that were obtained using the tomographic velocities from all of the models. The mispositioning of reflectors is obvious in the case of the isotropic assumption, but it is subtle in the anisotropic models.

Quantitative measures were made by measuring the differences between top salt horizon picks that came from

the actual model and those that came from the tomographic models. In figure 9, we can see the misties distributions for all the models statistically by the histograms. The followings are the mean of the absolute misties values and the standard deviation of the misties relative to perfect match for all of the models; 21 m and 26 for using Model 1, 30 m and 40 for using Model 2, 27 m and 34, for using Model 3, 26 m and 31 for using Model 4, and 64 m and 82 for using Model 5.

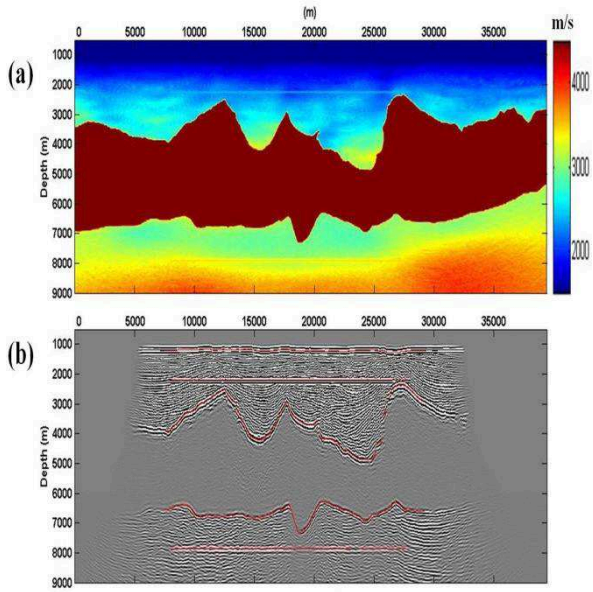

Figure 7: (a) Actual vertical velocity model. (b) migrated stack obtained by using the actual velocity model. Horizon picks from the actual velocity model are shown by red lines.

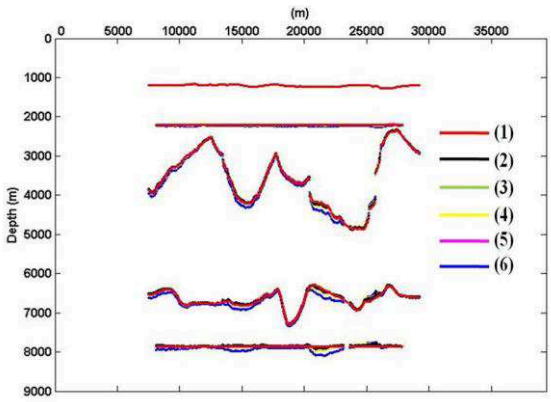

Figure 8: Horizons picks from actual velocity (1). Horizons picks from tomographic velocities using Model 1 (2), Model 2 (3), Model 3 (4), Model 4 (5), and Model 5 (6).

Although we used correct anisotropic model constraints, there are still errors in the resulting depth images, but clearly using the actual anisotropic model gives a smaller mistie range (less than 60 m) and mostly, they are distributed at around 20 m. Interestingly, the use of Model 4 gives a similar distribution range of misties as the use of the actual anisotropic model. The ε model trend of Model 4 is similar to the actual model, but with a slightly different scale. The δ of Model 4, on the other hand, is much different from the actual model. It appears that the δ has little effect on the tomography. Both the 2D interpolated anisotropic and the 1D anisotropic models give wider ranges of misties distributions. Isotropic model misties distribution is biased and large as we expected.

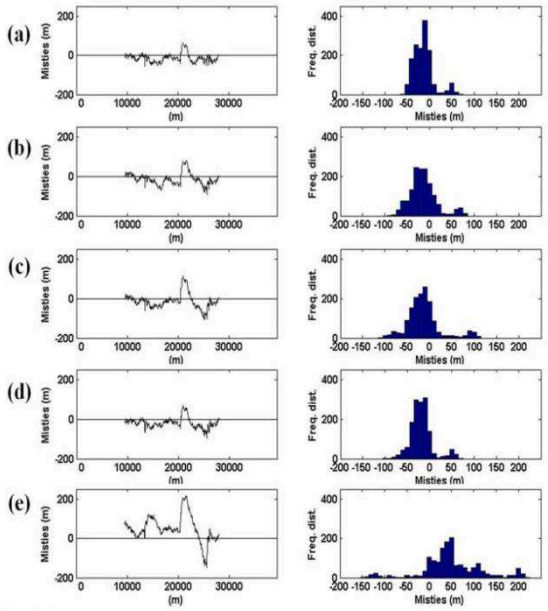

Figure 9 Left: misties of top salt horizon picks from actual velocity model and from tomographic velocity using (a) Model 1, (b) Model 2, (c) Model 3, (d) Model 4, and (e) Model 5. Right: Histograms of misties distribution correspond to the figures on the left.

Conclusion

Our conclusions are as follows:

1. Any anisotropic consideration is better than isotropic model.
2. In this case, the differences in accuracy of anisotropic model are not very large.
3. However, more precise anisotropic model constraints would still give better depth images especially for the subsalt target.

Acknowledgement

The authors acknowledge contributions of many colleagues in WesternGeco. We would like thank Dave Stathopoulos, Mita Sengupta and Arturo Ramirez for their valuable help and guidance, and the management of WesternGeco for permission to publish this work.

EDITED REFERENCES

Note: This reference list is a copy-edited version of the reference list submitted by the author. Reference lists for the 2010 SEG Technical Program Expanded Abstracts have been copy edited so that references provided with the online metadata for each paper will achieve a high degree of linking to cited sources that appear on the Web.

REFERENCES

Prioul, R., A. Bakulin, and V. Bakulin, 2004, Nonlinear rock physics model for estimation of 3D subsurface stress in anisotropic formations: Theory and laboratory verification: Geophysics, **69**, 415, doi:10.1190/1.1707061.

Sarkar, D., A. Bakulin, and R. L. Kranz, 2003, Anisotrpic inversion of seismic data for stressed media: Theory and physical modeling study of Berea sandstone: Geophysics, **68**, 690, doi:10.1190/1.1567240.

Sengupta, M., R. Bachrach, and A. Bakulin, 2009, Relationship between velocity and anisotropy perturbations and anomalous stress field around salt bodies: The Leading Edge, **28**, 598. doi:10.1190/1.3124936

Thomsen, L., 1986, Weak elastic anisotropy: Geophysics, **51**, 1954, doi:10.1190/1.1442051.

Woodward, J. M., D. Nichols, O. Zdraveva, P. Whitfield, and T. Johns, 2008, A decade of tomography: Geophysics, **73**, no. 5, VE5–VE11, doi:10.1190/1.2969907.